Chapter 2

# Mutation in *Mpzl3*, a Novel Gene Encoding a Predicted Adhesion Protein, in the rough coat (*rc*) Mice with Severe Skin and Hair Abnormalities

This chapter is based on:
Cao T, Racz P, Szauter KM, Groma G, Nakamatsu GY, Fogelgren B, Pankotai E, He QP, Csiszar K.. (2007) J Invest Dermatol.;127(6):1375-86.

## Abstract

The rough coat (*rc*), is an autosomal recessive mutation, arose spontaneously in C57BL/6J mice. Homozygous *rc* mice develop severe skin and hair abnormalities, including cyclic and progressive hair loss and sebaceous gland hypertrophy. The *rc* locus was previously mapped to Chromosome 9. To elucidate the genetic basis underlying the *rc* phenotype development, we carried out positional cloning and mapped the *rc* locus to a 246-kb interval. We identified a missense mutation within a novel open reading frame in the *rc/rc* mice, which is predicted to encode a cell adhesion molecule with the highest homology to Myelin Protein Zero (MPZ) and Myelin Protein Zero-like 2 (MPZL2, also called Epithelial V-like Antigen). We therefore named this gene *Mpzl3* (Myelin Protein Zero-like 3). The mutation in the *rc/rc* mice occurred at a highly conserved residue within the conserved immunoglobulin V-type domain, thus likely altering the MPZL3 protein function. Reverse transcriptase-PCR and Western blot analysis revealed expression of the *Mpzl3* gene in various adult organs, including the skin. Using indirect immunofluorescence, we detected MPZL3 protein in the keratinocytes and sebocytes in the skin. Results from this study identified a novel gene encoding a predicted adhesion protein whose mutation in the *rc* mice likely caused the *rc* phenotype.

## Introduction

The rough coat (*rc*) mutation arose spontaneously in the C57BL/6J (B6/J) inbred mouse strain at the Jackson Laboratory in 1966 (Dickie, 1966). The *rc* mutation is autosomal recessive. Homozygous *rc* mice are born with no apparent abnormalities, but display unkempt looking hair coats by weaning age, and develop cyclic and progressive hair loss thereafter (Figure 1) (Hayashi et al., 2004). In addition, histological analysis of skin sections revealed sebaceous gland hypertrophy in the *rc/rc* mice (Figure 2) (Hayashi et al., 2004; Ruvinsky et al., 2002). Both male and female homozygous *rc* mice are fertile (Dickie, 1966), although only about a quarter of the pups born to *rc*/*rc* females survive (Hayashi et al., 2004). Linkage analysis with DNA markers assigned the *rc* locus to 32.0 centimorgan on Chromosome 9, close to the *Mpi1* gene (2 recombinants among 107 backcross offspring) (Eicher EM, 1977) at 57.57 megabase (Mb) (Ensembl Mouse Genome Database v38, released in April 2006, www.ensembl.org/Mus_musculus), but the gene mutation remained unknown.

The appearance of rough hair coats in *rc/rc* mice is similar to matted (*ma*) mice, another strain with a spontaneous mutation (Searle AG, 1957). However, tests for allelism through breeding experiments with *ma* and several other mutant strains such as ichthyosis (*ic*), plucked (*pk*), fuzzy (*fz*) and rough (*ro*) (Dickie, 1966), abnormal feet and tail (*aft*) (Ruvinsky et al., 2002) have all been negative. Interestingly, mice homozygous for rough fur (*ruf*), another spontaneous mutation mapped to Chromosome 9, demonstrated similar skin abnormalities with the *rc/rc* mice, such

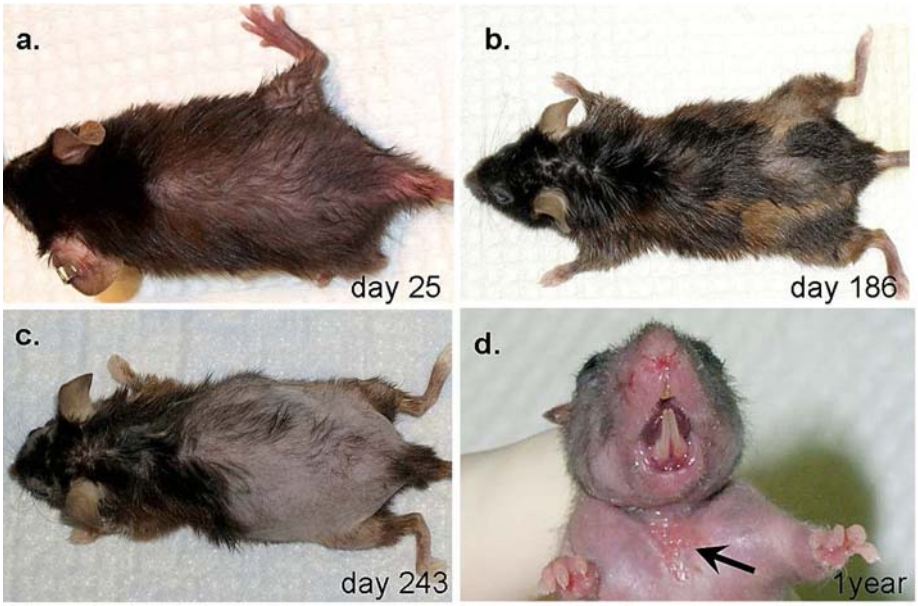


**Figure 1.** Gross phenotype of the *rc/rc* mice **(a)** Hair loss is apparent on the dorsal trunk of an rc/rc mouse on day 25 after birth. **(b)** New hair coat retains the rough coat phenotype, sometimes with reduced pigmentation. **(c)** Hair loss is progressive in older rc/rc mice. **(d)** In more than 50% of *rc/rc* mice older than 1 year, ulcerated wounds develop spontaneously in the ventral neck region (arrow).

as the "unkempt" and "wet" appearance and sebaceous gland hypertrophy (Park et al., 2001; Sweet HO, 1990). However, allelism has not been tested for *rc* and *ruf*, and the mutation in *ruf* mice has not been identified.

A previous study of the rough coat mutation (Hayashi et al., 2004) showed linkage of the *rc* locus with two microsatellite markers, *D9Mit162* at 49.954 Mb (one recombinant among 129 backcross offspring) and *D9Mit104* at 65.953 Mb (three recombinants among 129 backcross offspring). In this study, to elucidate the genetic basis and to better understand the molecular mechanisms of *rc* phenotype development, we carried out positional cloning in backcross mice.

## Results

### Cyclic and progressive hair loss and sebaceous hypertrophy in the *rc/rc* mice:

Homozygous *rc* pups were born with no apparent abnormalities, and developed normal hair coats that became plush 7 days after birth, suggesting that the initial hair growth (follicular neogenesis) in *rc*/*rc* pups was normal. However, by day 14 after

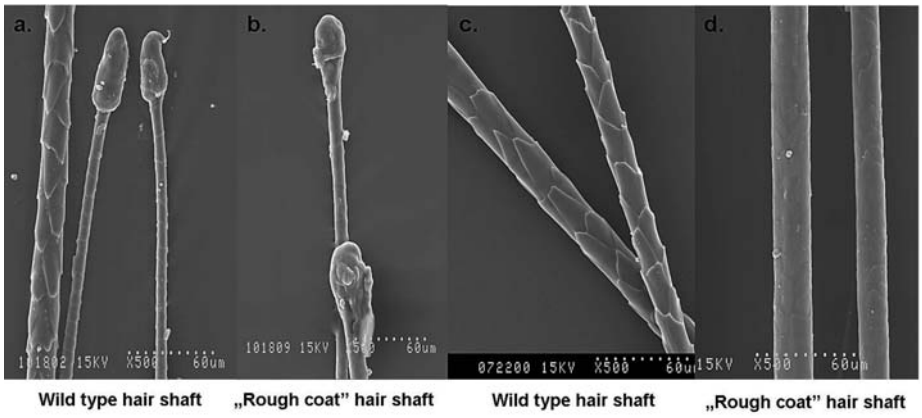


**Figure 2.** Ultrastructural analyses of hair shafts in *rc/rc* mice. Scanning electron microscopy images are shown of pelage hair from a 24 day old *rc/rc* mouse **(b, d)** and a wild type mouse **(a, c)**. Notice the smooth hair shaft **(d)** and abnormal hair bulb **(b)** from the *rc/rc* mouse. The presence of the hair bulb in **(b)** suggests that the hair loss in *rc/rc* mice is not due to breakage of hair. The smooth hair shafts of *rc/rc* mice **(d)** may result from the elevated level of sebum in the sebaceous glands.

birth, the *rc/rc* pups started to show unkempt-looking hair coats ("rough" coat) and a loss of glossiness. By day 18, hair loss became apparent on the dorsal, ventral, and lateral trunk. At the next anagen, the dorsal skin became dark and thickened, and the new hair coats retained the "rough coat" phenotype. Thereafter, the *rc/rc* mice underwent cyclic hair loss, and hair growth, sometimes showing reduced pigmentation in the new hair coat (Figure 1). Hair loss was progressive and some older *rc/rc* mice became nearly bald. In addition to hair loss, we observed a high incidence of spontaneous and persistent ulcerated lesions on the ventral skin of the neck in *rc/rc* mice over 1 year of age (17 of 27, 63%) (Figure 1d). Histological analysis of such lesions revealed typical features of chronic wounds, including inflammation in the wound bed and hyperplasia of the epidermal keratinocytes at the wound edge (Data not shown)

Scanning electron microscopy showed that *rc/rc* mice have smooth hair shafts compared to wild type mice (Figure 2a and 2b). No breakage of the hair shaft was observed in the *rc*/*rc* mice by scanning electron microscopy (Figure 2c and 2d), which supports that the hair loss phenotype is the consequence of deattachment of the hair bulbs and not due to loss of structural integrity of the hair shafts

We observed severe hypertrophy of the sebaceous glands in the skin sections from *rc*/*rc* mice at day 16 (Figure 3a and 3b). This observation was confirmed by oil red O staining of lipids in the cells of differentiated sebocytes (Figure 3c and 3d). Similar observations were made in *rc/rc* skin and at days 24, 34, and 76 (data not shown). Sebaceous gland hypertrophy was a result of sebocytes hyperplasia: there were twice as many sebocytes per sebaceous gland in *rc*/*rc* mice as in +/*rc* mice (14.9±2.8 vs.

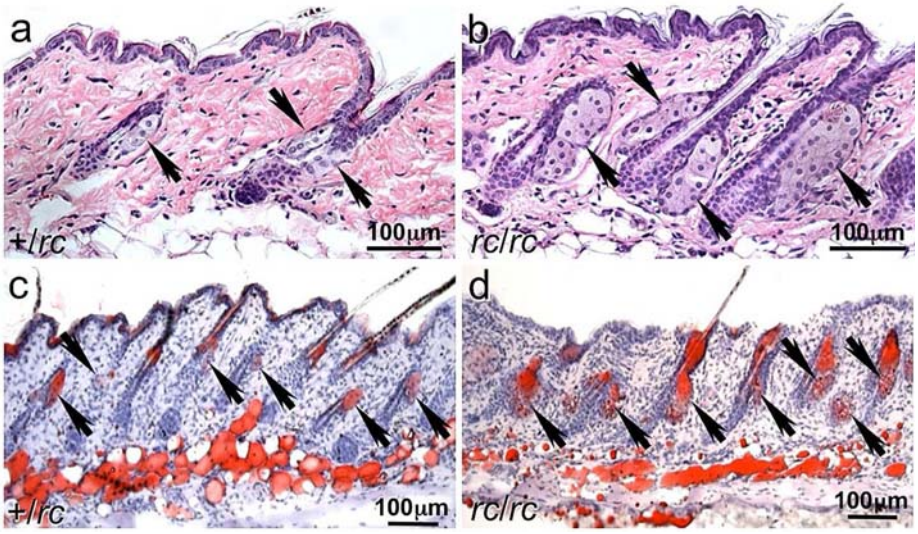


**Figure 3**. Sebaceous gland hypertrophy in the *rc/rc* mice. **(a, b)** Hematoxylin and eosin staining and **(c, d)** oil red O staining of lipids in back skin sections from **(a, c)** a +/rc and **(b, d)** an *rc/rc* mouse. Arrowheads point to the sebaceous glands. **(b, d)** Notice the hypertrophic sebaceous glands in the *rc/rc* mouse. The sebocytes **(d)** in the *rc/rc* mouse are functional lipid-secreting cells as **(c)** in the normal mouse. Bar = 100 mm

6.2±2.5 in the day 76 samples examined (P<<0.01). The smooth hair shafts observed in *rc/rc* mice (Figure 2) likely are the consequence of increased sebum production by the enlarged sebaceous glands.

## High-resolution linkage analysis:

Before this study, no mapping interval was defined for the *rc* locus, even though it had been mapped close to the *Mpi1* gene (Eicher EM, 1977) and two microsatellite markers, *D9Mit162* and *D9Mit104* (Hayashi et al., 2004). To define a mapping interval for the *rc* locus, we outcrossed B6/J-*rc*/*rc* mice with both CAST/Ei mice and BALB/cJ mice to obtain $F_1$ hybrids (+/*rc*) on two mixed strain backgrounds to avoid a potential low rate of recombination within the *rc* region (Fernandez-Gonzalez et al., 2002). Female $F_1$ hybrids were backcrossed with male B6/J-*rc*/*rc* mice to obtain $F_2$ hybrids.

We monitored $F_2$ hybrids daily from birth for the *rc* phenotype development. $F_2$ hybrids that showed unkempt hair coats by day 16, hair loss by day 24, ensuing hair growth, and subsequent hair loss were considered phenotypic and homozygous for the *rc* mutation (*rc*/*rc*). $F_2$ hybrids that never showed hair abnormality at these stages were considered non-phenotypic and heterozygous for the *rc* mutation (+/*rc*). Penetrance of the *rc* phenotype was 100% in both $F_2$ hybrid backgrounds.

**Table 1.** Summary of linkage analysis of five microsatellite marker and the rc locus in 200 C57BL/6J-BALB/cJ F2 offspring. p<<0.0001 for all markers.

| Marker | Position (Mb) | Number of Recombination | Number of Mice Analyzed | Distance (cM) | LOD score |
|---|---|---|---|---|---|
| D9Mit67 | 36.961 | 11 | 200 | 5.5 | 41.7 |
| D9Mit328 | 41.822 | 6 | 200 | 3 | 48.5 |
| rc | | | | | |
| D9Mit191 | 46.647 | 4 | 200 | 2 | 51.7 |
| D9Mit162 | 49.954 | 6 | 200 | 3 | 48.5 |
| D9Mit73 | 71.609 | 25 | 200 | 12.5 | 27.5 |

Mb: megabase. The Mb positions are based on the Ensembl Mouse Genome Database (http://www.ensembl.org/Mus_musculus), v38 (released in April 2006), based on the NCBI m35 assembly (released in December 2005). cM: centimorgan.

We analyzed linkage between the *rc* locus and five microsatellite markers in 200 B6/J-BALB/cJ $F_2$ hybrids (Table 1). Linkage was shown between the *rc* locus and all five microsatellite markers ($p<<0.0001$). All four recombinants with *D9Mit191* also showed recombination with *D9Mit162* and *D9Mit73*, and none of them showed recombination with *D9Mit67* or *D9Mit328*. All six recombinants with *D9Mit328* also showed recombination with *D9Mit67*, and none of them showed recombination with *D9Mit73*, *D9Mit162* or *D9Mit191*. These recombinations defined the *rc* interval between *D9Mit328* and *D9Mit191*.

Using a similar approach, we analyzed linkage between the *rc* locus and the published polymorphic microsatellites shown in Figure 4a in 361 B6/J-CAST/Ei $F_2$ hybrids. We were able to reduce the *rc* interval to 1.560 Mb, between *D9Mit228* and *D9Mit192*. We then identified eight novel microsatellite polymorphisms within the *D9Mit228~D9Mit192* interval between B6/J and CAST/Ei strains (Figure 4a). The chromosomal locations and primer sequences of these novel polymorphisms are shown in Table 2. Haplotype analysis of $F_2$ hybrids B292, B329 and B359 revealed that the *rc* locus lay within a 246-kb interval, between 44.8334 Mb (microsatellite # 9) and 45.0796 Mb (microsatellite #25) (Figure 4b).

## Mutation detection:

Within this 246-kb interval, there are 10 candidate genes, including nine known genes and one novel gene (Figure 4c). Using reverse transcriptase (RT)-PCR analyses, we detected expression of nine of the 10 candidate genes in normal as a well as *rc/rc* skin (data not shown). As we could not pinpoint a most likely "functional" candidate gene, such as one whose expression in the rc/rc skin was drastically down-regulated, we carried out sequence analyses of all the coding sequences and flanking splice sites of all 10 candidate genes. There are total of 71 exons among these genes, 68 of which contain coding sequences, according to the Ensembl Mouse Genome Database (www.ensembl.org/Mus_musculus). These numbers included all exons predicted from different transcripts in the Ensembl database (www.ensembl.org/

**Table 2.** Summary of linkage analysis of novel microsatellite polymorphisms we identified between B6/J and CAST/Ei strains and the rc locus in 361 C57BL/6J-CAST/Ei F2 hybrids.

| Marker | Chromosomal Position (Mb) | Number of Recombinants | Primer Sequences |
|---|---|---|---|
| # 3 | 44.4246 | 1 | F: CTGGCTCTACAGGCGTGTAC<br>R: TGCTAAGTAAGGAGAGAGGG |
| # 5 | 44.4827 | 1 | F: TGATCTCCTGGTCCCATGAG<br>R: GGATCCACTTGTAAATGTGC |
| # 14 | 44.6485 | 1 | F: CTCTGCTCTCCACACTCATC<br>R: TGCACACGCTTGTGACCATG |
| # 7 | 44.8185 | 1 | F: TCAATGGGAGAGTGCTTGCC<br>R: GAATCTCTCTCAGTGCCTCC |
| # 9 | 44.8334 | 1 | F: GGAGAGTGAGAAAGCAGGAC<br>R: CCCTAGCCTATGAGATCTCC |
| # 10 | 44.8827 | 0 | F: AGGTTTTGTAGAATCCAGGC<br>R: CTGACCTCCACACTACACTC |
| # 25 | 45.0796 | 1 | F: TCACAGACATGGCAGGAGTC<br>R: CCTCTGCTTCTGGTTGCTAC |
| # 26 | 45.1235 | 1 | F: GGCTAATTCAGCGTACACAC<br>R: CTCAGGTCATTTGGCACCAG |

Mb: megabase. The Mb positions are based on the Ensembl Mouse Genome Database (http://www.ensembl.org/Mus_musculus), v38 (released in April 2006), based on the NCBI m35 assembly (released in December 2005).

Mus_musculus, NCBI m35 assembly released in December 2005, with reference to NCBI m36 assembly released in April 2006). We did not identify any mutation in the known genes in the *rc/rc* DNA.

However, we identified a point mutation in the open reading frame within the novel gene ENSMUSG00000070305, located at 44.989~45.009 Mb (Figure 5, Table 3). This novel gene consists of six exons, and encodes a polypeptide, ENSMUSP00000091378, of 230 amino acids. A closer examination revealed that the coding sequence did not start with an ATG nor ended with a STOP codon. We therefore considered it incomplete. This novel gene has a human homologue ENSG00000160588 at 117,602,619 ~ 117,628,245 bp on Chromosome 11, and a rat homologue ENSRNOESTG00000015598 at 48,004,303 ~ 48,024,405 bp on Chromosome 8. The human homologue and rat homologue encode polypeptides of 235 (ENSP00000278949) and 236 (ENSRNOESTP00000021062) amino acids, respectively. By comparison with the human and rat homologues and analyses of the mouse genomic sequence and expressed sequence tags (ESTs), we predicted additional four amino acids at the amino and carboxyl termini of the encoded mouse polypeptide. There are additional four amino acids at the amino terminus, starting with a methionine encoded by ATG. We also identified an in-frame STOP codon 36 bp upstream from this ATG within the 5' flanking sequence. Furthermore we predicted an additional three amino acids at the carboxyl terminus, followed by a STOP

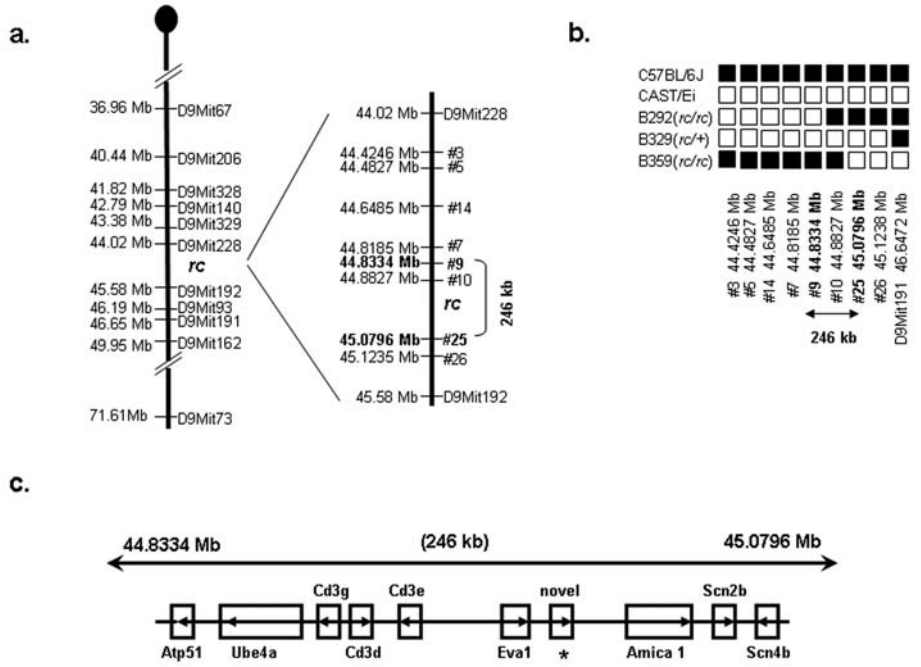


**Figure 4**. High-resolution genetic map of the *rc* interval and the candidate genes. **(a)** High-resolution genetic map of the *rc* interval based on linkage analysis in 200 C57BL/6J-BALB/cJ and 361 C57BL/6J-CAST/Ei F2 hybrid offspring. Microsatellite markers in the Ensembl Mouse Genome Database (http://www.ensembl.org/Mus_musculus) are shown on the left with their chromosomal locations in megabases (Mb). Novel microsatellite polymorphisms between the C57BL/6 and CAST/Ei strains identified in this study are shown on the right. Marker #10 was concordant with *rc* in all the F2 hybrids we analyzed, and its location relative to the *rc* locus could not be determined in our linkage analysis. **(b)** Haplotype analysis of the three recombinants with D9Mit191 or marker #3 among the 361 C57BL/6J-CAST/Ei F2 hybrid offspring. These results show that the rc locus lies within a 246-kb interval. **(c)** Candidate genes in the 246 kb mapping interval for the *rc* locus (Ensembl Mouse Genome Database, www.ensembl.org/Mus_musculus).

codon. Thus, we predicted a polypeptide of 237 amino acids encoded by the mouse gene ENSMUSG00000070305. We have submitted this novel gene/mRNA sequence to GenBank (GenBank accession number EF102773).

The mutation we identified in the *rc/rc* DNA is a G→A transition in exon 3 of this gene, resulting in an, Arg100→Gln substitution, in the predicted 237-amino acid polypeptide (Figure 5). This mutation was confirmed in multiple *rc/rc* mice of different parents and in *rc*/+ mice, as well as in C57BL/6J-*rc* genomic DNA purchased from the Jackson Laboratory (Bar Harbor, ME).

To determine whether this mutation could be a polymorphism, we carried out

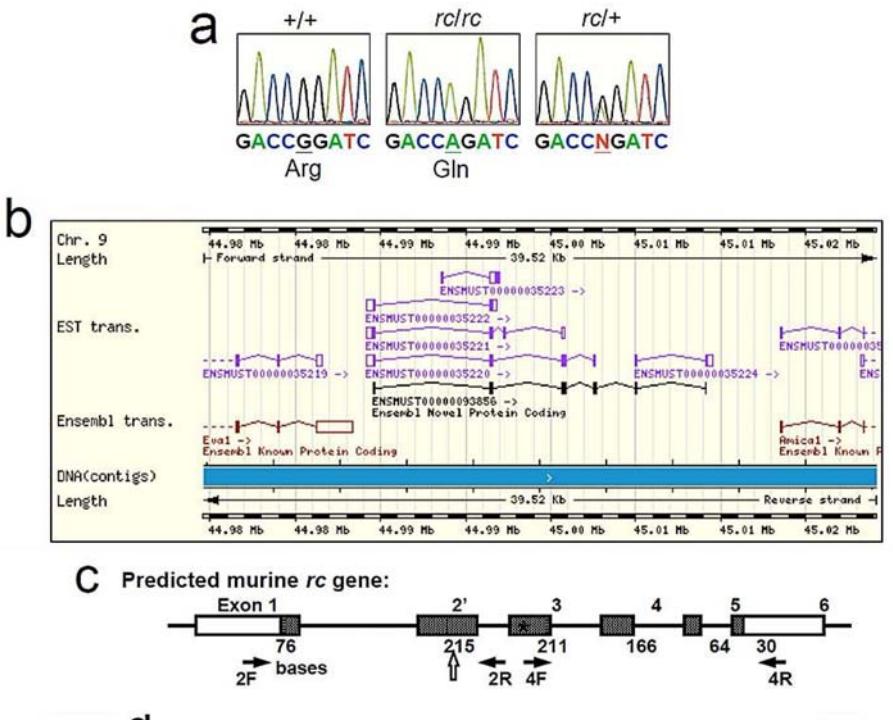


d

| Exons | Exon Size (bp) | 5' Splice Donor Sequence | Intron Size (bp) | 3' Splice Acceptor Sequence |
|---|---|---|---|---|
| 1 | Noncoding + 76 | TCCAGG**gt**gagt | 6,722 | c**attag**GTGCGC |
| 2 | 167 | GAGTCT**gt**gagt | 4,131 | tc**ttag**ATTTTT |
| 2' | 215 + noncoding | - | - | - |
| 3 | 211 | AAAGGG**gt**aagc | 1,657 | c**tacag**GGTTCG |
| 4 | 166 | CGATGA**gt**aagt | 2,283 | c**cacag**CACTGA |
| 5 | 64 | TGTCTG**gt**aagt | 4,034 | c**tctag**GATTCA |
| 6 | 30 + noncoding | | | |

**Figure 5**. Gene structure and mutation analysis of a novel gene in which a mutation was identified in the *rc/rc* DNA. **(a)** Sequence analysis identified a point mutation in a predicted open reading frame in the *rc/rc* genomic DNA, which was confirmed in *rc*/+ genomic DNA and *rc/rc* cDNA. We have named this gene "*Mpzl3*" based on the similarity of the predicted domain structure of its encoded protein to Myelin Protein Zero (MPZ) and Myelin Protein Zero-like 2 (MPZL2, also called EVA1). **(b)** The *Mpzl3* gene (ENSMUSG00000070305), predicted on the basis of multiple Ensembl transcripts based on ESTs, in its genomic context. *Eva1* (*Mpzl2)* gene is upstream, and *Amica1* gene is downstream. **(c)** Our prediction of the murine *Mpzl3* gene that is homologous to the human gene ENSG00000160588 and rat gene ENSRNOESTG00000015598. Exon and EST information was based on the Ensembl Genome Database (www.ensembl.org) and our prediction by sequence

comparison between species. Numbers underneath each exon indicate the length of the coding sequence in that exon (shaded portion). Exon 2 has 167 bp of coding sequence, and exon 2′ has 215 bp of coding sequence (48 bp longer than exon 2) as well as a 3′ UTR. Block arrow points to the splice site in exon 2′ used to generate the 6-exon transcript. The arrows denote primers 2F, 2R, 4F and 4R used for RT-PCR analysis in Figure 6. The asterisk (*) denotes the position of the mutation detected in *rc/rc* DNA. **(d)** Exon-intron information of the predicted murine *Mpzl3* gene.

sequence analysis of this gene in multiple mouse strains. This mutation was absent in wild type Balb/c, CAST/Ei, B6C3F1 (F1 hybrid of C57BL/6NCr and C3H/HeN MTV-), B6D2F1 (F1 hybrid of C57BL/6NCr and DBA/2NCr), CD1, and SwissGP mice.

The protein encoded by the mutated gene:

According to our prediction based on homology to human and rat counterparts, the full length polypeptide encoded by the murine ENSMUSG00000070305 gene consists of 237 amino acid residues, and has a predicted molecular weight of 26,058 Dalton and isoelectric point of 7.73. It is predicted to be a type I transmembrane protein, with a signal peptide at the amino terminus (amino acids 1~32), an immunoglobulin (Ig)-like V-type domain at amino acids 33~149, and a transmembrane domain at amino acids 160~182 (Figure 6). The Ig-like V-type domain is predicted to be extracellular upon cleavage of the signal peptide, and the carboxyl terminus is predicted to be cytoplasmic. The conserved cysteines in the Ig-like domain are at amino acids 53 and 129, and there is a putative N-glycosylation site (NXS/T) at amino acid 124. Arg100 is a highly conserved residue within the Ig domain.

Among known murine proteins, the highest sequence homology to this 237-amino acid protein was identified in the Myelin Protein Zero (MPZ) and Myelin Protein Zero-like 2 (MPZL2, also called Epithelial V-like Antigen, (EVA1)) (Figure 6). We therefore registered this novel gene as *Mpzl3* (Myelin Protein Zero-like 3) with the International Committee on Standardized Genetic Nomenclature for Mice and the Mouse Genomic Nomenclature Committee (MGNC) through the Mouse Genome Informatics (MGI) Resource (The Jackson Laboratory, Bar Harbor, ME). Both MPZ and MPZL2 (EVA1) proteins have been implicated in cell-cell adhesion (Guttinger et al., 1998), and the Ig-like domains in a number of other proteins have been shown to mediate homophilic cell-cell adhesion. Hence, it is likely that the MPZL3 protein is also involved in cell adhesion through its immunoglobulin V-type domain, and that substitution of the highly conserved Arg100 alters its function.

The coding sequence of the six-exon murine *Mpzl3* transcript shares an 84.5% nucleotide identity with its human homologue, and the murine and human MPZL3 proteins share an 86.8% identity and 93.2% similarity. However, within the conserved Ig-like V-type domain, the murine and human MPZL3 proteins share a 93.3% identity and 96.6% similarity. The coding sequence of the six-exon murine *Mpzl3* transcript shares a 93.3% nucleotide identity with its rat homologue, and the murine and rat MPZL3 proteins share a 96.6% identity and 97.9% similarity. Interestingly, EST evi-

**Table 3.** Sequences of primers used to PCR amplify the six exons of the novel mouse gene ENSMUSG00000070305 (later named Mpzl3) for sequence analysis.

| Exons | Forward Primer | Reverse Primer | Amplicon (bp) |
|---|---|---|---|
| Exon 1 | ATCAGATCCTCCTGAGAGTC | TCAAGTCTCACAAGGTGGTC | 518 |
| Exon 2/2' | TGAAGCATCTCTCATGTTCAC | AAACTTGCACAGCAGGTGAC | 433 |
| Exon 3 | ACAGCCAAGGGAAGAGAAGC | ACCTTGACACAGTGATCCTC | 422 |
| Exon 4 | CTTTTACGAACATGCGTCCTG | TCAGCAGTGGACCAAACGTC | 441 |
| Exon 5 | GCTCCGATATGTGCTTCACG | GTTCATACGTTCCTGTGCTG | 307 |
| Exon 6 | GAGCATAGGTGTGCTCTCAG | GATCTTCTGTCACTGCTGTC | 267 |

The reverse primer for exon 2/2' was also used to PCR amplify the two-exon Mpzl3 cDNA (primer 2R in Figure 5c).

dence also suggests a two-exon *Mpzl3* transcript in mice (ENSMUST00000035222) and rats (ENSRNOT00000032837), encoding a polypeptide of 96 amino acids. The 96-amino acid mouse and rat polypeptides are highly homologous, with 90.6% identity and 95.8% similarity.

A search of the available genome databases showed MPZL3 homologues in human, chimpanzee, rhesus monkey, rat, mouse, bovine, dog, and opossum. In all of these organisms, Arg100 is highly conserved. However, the function of the MPZL3 protein is not known in any of these organisms.

## The murine *Mpzl3* gene:

The murine *Mpzl3* gene consists of six exons, spanning over 19 kb on mouse Chromosome 9 (44.989 ~ 45.010 Mb) (Ensembl v38; Vega release 18, May 08, 2006) (Figure 5b). According to our prediction based on homology to human and rat counterparts, the coding sequences in the murine *Mpzl3* exons varied from 30 bp (exon 6) to 215 bp (exon 2'), and the introns varied from 1,657 bp (intron 3) to 6,722 bp (intron 1) (Figure 5c, 5d). EST analysis provided evidence for at least two transcripts through alternative splicing, both containing coding sequences flanked by a 5' UTR that included an in-frame STOP codon and a 3' UTR. One transcript consisted of two exons encoding a polypeptide of 96 amino acids. EST evidence suggested a 5' UTR of at least 53 bp and a 3' UTR of at least 3,160 bp for this transcript. This transcript, however, does not contain a mutation. Interestingly, there is a consensus splice donor site within the coding sequence of exon 2' (Figure 5d). When this site is used, a transcript containing six exons would result from the *Mpzl3* gene, encoding a protein of 237 amino acids. EST evidence suggested a 5' UTR of at least 57 bp and a 3' UTR of at least 261 bp for this transcript. In the *rc/rc* mice, the G→A missense mutation we identified in exon 3 would result in Arg100→Gln substitution.

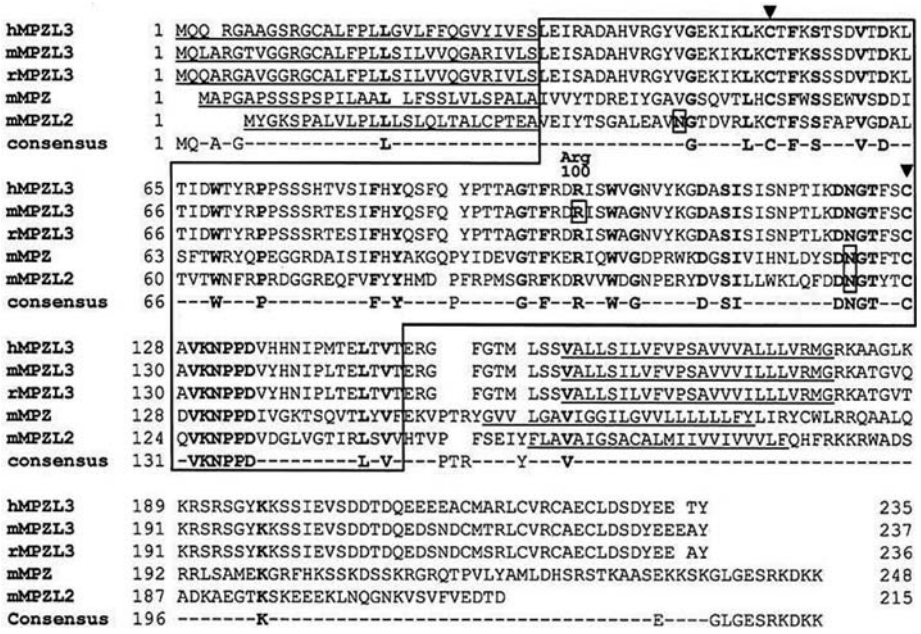


**Figure 6**. Sequence comparison of the human, murine, and rat MPZL3 protein and murine MPZ and MPZL2 (EVA1). The signal peptides and trans-membrane domains are underlined, flanking the immunoglobulin (Ig)-like V-type domains, with conserved residues highlighted. "N" over grey background: N-linked glycosylation site; "C" over grey background: conserved "signature" Cysteines for disulfide bond formation in the Ig-like domain. The Arginine (R) 100→glutamine (Q) substitution caused by the G→A mutation in the *rc/rc* mice is highlighted over grey background

## Expression of the *Mpzl3* mRNA:

We carried out RT-PCR analysis to determine the tissue distribution of the *Mpzl3* transcripts in normal adult mice. Primers were designed to amplify the complete coding sequences from both the six-exon (845 bp amplicon using primers 2F and 4R) (Figure 5c) and two-exon (457 bp amplicon using primers 2F and 2R) (Figure 5c) transcripts based on EST predictions. As shown in Figure 7a, the two *Mpzl3* transcripts were detected in a variety of organs examined, with high levels of expression in the brain, heart, liver, and skin. The tissue distribution patterns of the two-exon and six-exon transcripts were similar.

RT-PCR analysis also showed *Mpzl3* transcripts expression in the *rc/rc* mouse skin (Figure 7b). We sequenced the RT-PCR products from both normal and *rc/rc* skin complementary DNA (cDNA), and confirmed the G→A mutation in exon 3 of *Mpzl3* in the *rc/rc* cDNA derived from the 6-exon transcripts.

To detect the MPZL3 protein, we generated affinity purified rabbit polyclonal antibodies against a peptide (DKLTIDWTYRPPSSSRT) in the predicted extracellular domain of the murine MPZL3 protein. To test the specificity of these antibodies,

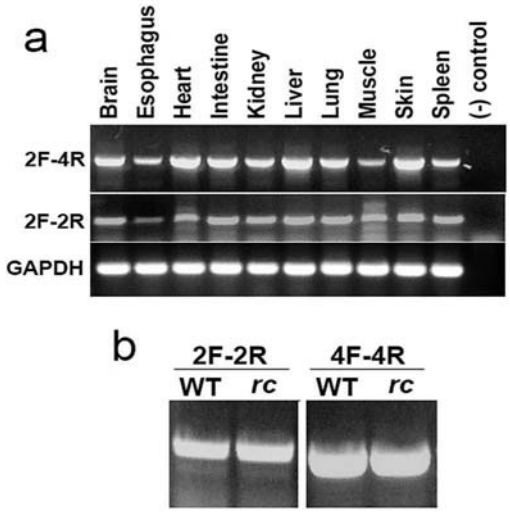


**Figure 7**. RT-PCR analysis of *Mpzl3* gene expression. **(a)** Expression of the 6-exon *Mpzl3* transcripts (2F-4R) and the 2-exon *Mpzl3* transcripts (2F-2R) in normal adult mouse organs. The two transcripts had similar tissue distribution. **(b)** Expression of the 6-exon *Mpzl3* transcripts (4F-4R to amplify exons 3~6) and the 2-exon *Mpzl3* transcripts (2F-2R) in wild type (WT) and *rc/rc* mouse skin.

we transfected NIH/3T3 cells with an expression vector encoding a fusion protein between the murine MPZL3 and Myc epitope tag. We analyzed total cell extracts by western blot analyses using the anti-MPZL3 antibodies, detecting two bands at approximately 27 and 29 kDa (Figure 8a). These bands were also recognized by the anti-Myc antibody (Figure 8b). The size difference may be due to different post transcriptional modifications. when the anti-MPZL3 antibodies were preabsorbed with the DKLTIDWTYRPPSSSRT peptide at a 1:3, 1:10, or 1:32 molar ratio, binding to the fusion protein became much weaker at 1:3 molar ratio (Figure 7c; very faint band s at 27 and 29 kDa were visible with much longer exposure, data not shown) and could not be detected at a 1:10 (Figure 8d) or 1:32 molar ratio (data not shown). These result suggest that the anti MPZL3 antibodies specific for the antigen. The anti MPZL3 antibodies also detected 27 and 29 kDa bands in NIH/3T3 cells transfected with a plasmid encoding the *rc* mutant MPZL3 protein fused to the Myc tag (data not shown) as expected. In addition, using the anti-MPZL3 antibodies, we detected bands that were of much higher molecular weight (~80 and ~110kDa), which were not detected with preabsorbed anti-MPZL3 antibodies or the anti-Myc antibody (Figure 8a-d). These bands could be endogenous MPZL3 with different post-transcriptional modifications or from different transcripts.

In all the adult mouse organs analyzed by Western blot, we detected a single band at approximately 70 kDa (Figure 8e) When we used preabsorbed antibodies to analyze skin and kidney extracts, we detected no signal (data not shown) suggesting the antibody binding was specific. The band detected is much larger than the size predicted from the amino-acid sequence (237 amino acids before the cleavage of predicted signal peptide), which may result of post-transitional modification, such glycosylation or dimerization or from translation of different transcripts. Interestingly, the bands detected in NIH/3T3 cells (~80 and ~110 kDa) were not detected in any

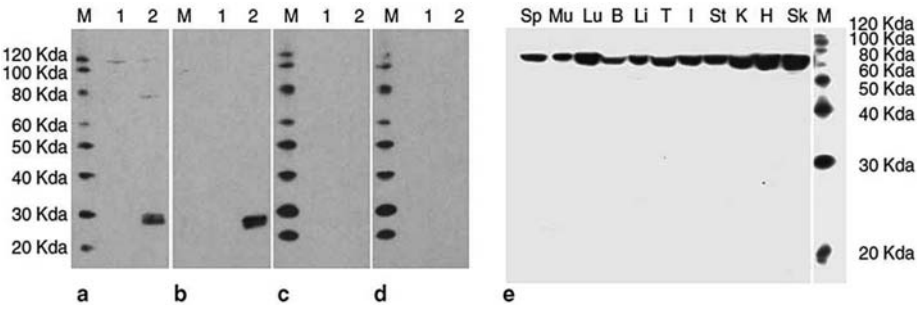


**Figure 8**. Characterization of the anti-MPZL3 antibodies and expression of MPZL3 in adult mouse organs. **(a–d)** Western blot analysis of total cell extracts from control NIH/3T3 cells **(lane 1)** and NIH/3T3 cells transfected with pEF/myc/cyto containing wild-type murine Mpzl3 cDNA **(lane 2)**. The primary antibodies used were: **(a)** rabbit anti-MPZL3 peptide DKLTIDWTYRPPSSSRT affinity-purified antibodies**, (b)** mouse anti-Myc tag antibody, rabbit anti-MPZL3 affinity-purified antibodies preabsorbed with **(c)** 1:3 or **(d)** 1:10 molar ratio of peptide DKLTIDWTYRPPSSSRT. Blot c showed very faint bands of 27 and 29 kDa after a much longer exposure (data not shown). **(e)** Western blot analysis of total protein extracts from adult mouse organs detected by rabbit anti-MPZL3 affinity-purified antibodies. Sp: spleen; Mu: muscle; Lu: lung; B: brain; Li: liver; T: testis; I: intestine; St: stomach; K: kidney; H: heart; Sk: skin. M: MagicMark XP.

mouse organs analyzed, suggesting they may unique for cultured NIH/3T3 cells.

We were interested to determine MPZL3 protein expression and localization in the skin, therefore we carried out indirect immunofluorescence of adult mouse skin sections. We detected MPZL3 expression in keratinocytes of the epidermis and hair follicles (Figure 9). By examining staining at high magnifications, it was clear that the staining was strong around the plasma membrane (Figure 9e and f), consistent with the prediction of a transmembrane protein involved in cell adhesion. We also detected staining in the cytoplasm, but not in the nuclei. We did not detect differences in the MPZL3 protein distribution pattern between normal and *rc/rc* mouse skin. Using *rc/rc* skin sections with hypertrophic sebaceous glands, we also detected MPZL3 expression in the sebocytes (Figure 9c, d, and g). As a negative control, indirect immunofluorescence using normal goat serum instead of anti-MPZL3 antibodies did not show any specific staining (data not shown).

## Sequence analysis of the *Mpzl3* gene in *ruf/ruf* mice:

The *ruf/ruf* mice develop skin abnormalities similar to the *rc/rc* mice, such as "unkempt" and "wet" looking hair coats and sebaceous gland hypertrophy (Park et al., 2001), and the locus has been mapped to Chromosome 9 (Sweet HO, 1990). Although allelism between these two spontaneous mutations has not been tested directly, it is possible that they are caused by mutations in the same gene. However, our sequence analysis of the *Mpzl3* gene coding sequences did not detect any differ-

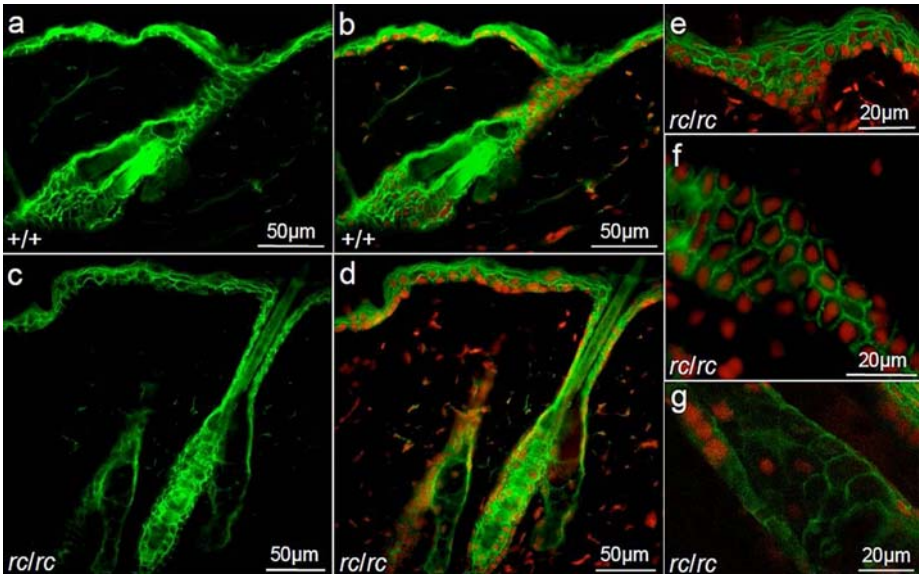


**Figure 9**. Expression of MPZL3 in mouse skin sections detected by indirect immunofluorescence. **(a–f)** MPZL3 (green) was detected in the keratinocytes of the epidermis and hair follicles as well as **(a–d, g)** the sebocytes. **(b, d–g)** Sections were counterstained with propidium iodide (red). **(a, b)**: +/+ skin; (c–g): *rc/rc* skin. Bar¼50 mm in **(a–d)**, 20 mm in **(e–g)**.

ence between the parental C3H/HeJ and *ruf/ruf* genomic DNA purchased from the Jackson Laboratory (Bar Harbor, ME). Therefore, our results suggest that *ruf* and *rc* are likely not allelic.

## Discussion

In this study, we carried out positional cloning of the gene mutated in the *rc* mice. We mapped the *rc* locus to a 246-kb interval by high-resolution linkage analysis, and identified a missense mutation which resulted in an Arg100→Gln substitution in a novel open reading frame within this interval. Based on the predicted domain structure of the encoded protein, we named this novel gene *Mpzl3* encoding a full-length MPZL3 polypeptide of 237 amino acids. Arg100 is a highly conserved residue within the conserved Ig-like V-type domain. Therefore, substitution of Arg100 is highly likely to alter the MPZL3 protein function in the *rc/rc* mice.

### The MPZL3 protein:

Through BLAST search, the highest levels of sequence homology with the MPZL3 protein were identified in the Myelin Protein Zero (MPZ) and MPZL2 (Myelin Protein Zero-like 2, also called EVA1) proteins (Figure 6). Within the Ig-like V-type

domain, however, the MPZL3 protein shares a 40.0% identity and 54.2% similarity at the amino acid level with MPZ, and a 36.1% identity and 60.5% similarity at the amino acid level with EVA1. All the consensus residues within the Ig V-type domain, such as the cysteines and the N-glycosylation site, as well as the Arg corresponding to Arg100 in the MPZL3 protein, are conserved between these three proteins. Interestingly, the *Mpzl3* gene is located approximately 1 kb 3' to the *Eva1* gene, and the sizes of exons 2 and 3 are identical (167 bp and 211 bp, respectively). It is possible that these two genes arose through tandem duplication.

Whereas the *Mpzl3* gene encodes a short peptide of 96 amino acids through an alternatively spliced transcript in both mice and rats, there is no EST evidence that such a transcript exists in humans. Both the mouse and rat 96-amino acid polypeptides possess a signal peptide but have only a portion of the Ig-like domain, and lack a transmembrane domain downstream. In addition, EST evidence suggests the existence of other forms of *Mpzl3* transcripts (Figure 5b). It is not known whether such transcripts are expressed at significant levels in mice and rats, and the subcellular location and possible functions of the encoded polypeptides remain to be determined.

## The *rc* mutation:

The *rc* mutation arose spontaneously without mutagens in 1966, and all the allele has been maintained in cryopreserved embryos during most of the past four decades. Hence we expected a "simple" mutation without gross chromosomal rearrangement (such as those induced by X-ray irradiation). It is therefore not surprising that we detect a single nucleotide transition, which resulted in an amino –acid substitution. The mutated *Mpzl3* transcripts and protein were detected at significant levels in the skin of *rc/rc* mice, suggesting that the effect of the mutation is likely posttransitional. Substitution of the highly conserved Arg100 in the conserved Ig-like domain required for adhesion may result in decreased cell adhesion. Shedding of hair at the telogen phase in the *rc/rc* mice may be one of the effects of such reduced adhesion.

In this study, we did not detect any mutations/polymorphisms in the *Mpzl3* gene in other mouse strains we analyzed. However, there are at least five documented variations in the mouse *Mpzl3* gene between mouse strains: four of them being synonymous, and one being non-synonymous. This non-synonymous polymorphism results in an Ala27→Val substitution within the signal peptide in the 129X1/SvJ strain, and likely has no functional consequence on the mature protein, as the mice appear normal.

The abnormalities in the *rc/rc* mice are not limited to the skin (Hayashi et al., 2004), and the mutated gene likely plays a role in the normal functioning of multiple organ systems. Not surprisingly, the *Mpzl3* transcripts were detected in a variety of organs. However, no other alleles of the *Mpzl3* mutation have been described. It is possible that the mutation we identified in the *rc/rc* mice is a "hypomorph". A more drastic change in the *Mpzl3* gene, such as a large deletion or early frame-shift muta-

tion, may lead to much more severe abnormalities in other organ systems and result in a lethal phenotype, and would therefore have never been documented as a natural mutation. Future functional analyses such as knock-out or knock-down experiments will be able to address such a possibility.

Mutations in adhesion molecules:

Mutations in a number of genes involved in cell adhesion, particularly components of the desmosomes, both transmembrane and intracellular, have been associated with defects of the skin and heart, where there are high levels of mechanical stress (McMillan and Shimizu, 2001). The *Mpzl3* gene expression was detected at high levels in the skin and heart, where the *rc/rc* mice develop severe abnormalities (Hayashi et al., 2004), and the MPZL3 protein is localized to the plasma membrane, consistent with the assumption that the MPZL3 protein may be involved in cell adhesion. Whereas there have been no reports of mutations in the *MPZL2* (*EVA1*) gene in human diseases, substitutions of conserved residues such as Thr124→Met in the Ig domain in the MPZ protein have been identified in patients with Charcot-Marie-Tooth disease (Chapon et al., 1999; De Jonghe et al., 1999; Misu et al., 2000). Similarly, substitution of the highly conserved Arg100 with Gln in the Ig domain of the MPZL3 protein likely results in alteration of the protein function in the *rc/rc* mice.

Interestingly, transgenic mice over-expressing c-*myc* in the keratinocyte stem cells also show sebaceous hypertrophy, hair loss, and spontaneous wounds (Arnold and Watt, 2001; Frye et al., 2003; Waikel et al., 2001) , though not as severe. In addition, while the effects of over-expressing c-*myc* were dominant, the effects of *rc* mutation were recessive. Over-expression of c-*myc* has been shown to drive the KSCs out of the stem cell compartment (Arnold and Watt, 2001; Waikel et al., 2001), and gene expression profiling has revealed that 40% of all down-regulated genes in the c-*myc* transgenic mice encoded cell adhesion molecules or cytoskeleton proteins, resulting in the reduced adhesive interactions of KSCs with the local microenvironment or niche. In addition, the failure of hair differentiation of the c-*myc* transgenic mice may reflect an inability of keratinocytes to migrate along the outer root sheath to receive hair inductive stimuli (Frye et al., 2003). It is therefore possible that the *Mpzl3* leads to similarly compromised interactions of the keratinocytes with their microenvironment and manifestation of the *rc* phenotype.

## Materials and methods

Mice:

All animal procedures were approved by the University of Hawaii Institutional Animal Care and Use Committee (IACUC). Mice were maintained in a temperature-, humidity-, and light cycle (12:12) controlled vivarium under specific pathogen-free conditions. One male and three female heterozygous rough coat (+/*rc*) mice in the C57BL/6J (B6/J) strain background were purchased from the Jackson Laboratory

(Bar Harbor, ME) to establish our own rough coat mouse colony. Female BALB/cJ and CAST/Ei mice were also purchased from the Jackson Laboratory for backcross studies.

## Histological analysis:

The dorsal skin of euthanized B6/J-*rc*/*rc* and age- and sex-matched B6/J-+/*rc* mice was shaved, and skin biopsies were collected. They were embedded in OCT or fixed in phosphate-buffered formalin and dehydrated and cleared in xylene before being embedded in paraffin. The cryosections were stained with oil red O for lipids, and the paraffin sections were stained with hematoxylin and eosin. Ultrastructural analyses were made using a Hitachi S-4800 Field Emission Scanning Electron Microscope with Oxford INCA X-Act EDS System.

## Backcross:

B6/J-*rc*/*rc* mice were outcrossed with both female BALB/cJ and CAST/Ei mice to obtain $F_1$ hybrids (+/*rc*). Because female *rc*/*rc* mice do not breed well (Hayashi et al., 2004), we used male B6/J-*rc*/*rc* mice and $F_1$ females for our backcross experiment to obtain $F_2$ hybrids for linkage analysis.

## Genotyping:

Genomic DNA of $F_2$ hybrids was extracted from tail tip biopsy at the time of weaning using Proteinase K (Invitrogen Corporation, Carlsbad, CA) digestion and ethanol precipitation. PCR reactions were carried out to amplify microsatellites polymorphic between the parental strains, and the amplified DNA fragments (amplicons) were analyzed using 4% Metaphor agarose (Cambrex, Rockland, ME) gel electrophoresis. In cases when there were no more published microsatellite polymorphisms between the parental strains in the Mouse Genome Informatics "Strains and Polymorphisms" database (www.informatics.jax.org) or the Ensembl Mouse Genome Database (www.ensembl.org/Mus_musculus), we designed primers to detect novel polymorphisms between B6/J and BALB/cJ or between B6/J and CAST/Ei. Microsatellites with at least 15 CA or TG repeats based on sequence information in the Ensembl Mouse Genome Database (C57BL/6 strain) were amplified by PCR from these strains and the amplicons were analyzed by agarose gel electrophoresis. Those with detectable polymorphisms (at least 8 bp on a 4% Metaphor agarose gel) were used for linkage analysis.

## Linkage analysis:

Backcross offspring were scored for recombination events that segregate the microsatellite markers contributed by the two parental alleles and the *rc* locus (indicated by the phenotype). The distances between the loci and the LOD scores were calculated using the QTXb20 software(Manly et al., 2001) .

## Mutation detection:

Primers for sequence analysis were designed based on the C57BL/6 genomic sequence and exon structure in the Ensembl Mouse Genome Database (www.ensembl.org/Mus_musculus). Primers were located in the introns, 5' and 3' UTRs or 5' and 3' flanking sequences so that mutations in the exon sequence as well as the splice donor, acceptor, and branch sites could be detected. Primers were synthesized at Integrated DNA Technologies (Coralville, IA), and PCR reactions were carried out using both wild type B6/J and B6/J-*rc*/*rc* mouse genomic DNA as templates. The amplicons were analyzed by agarose gel electrophoresis, and the DNA was recovered from the gel using GeneClean Spin Kit (Q-Biogene, Carlsbad, CA). Sequences from both strands were obtained BigDye sequencing kit and an ABI PRISM 3100 Genetic Analyzer (Applied Biosystems, Foster City, CA) at sequencing core facilities (MBSR, CGPBRI, and GMBF) at University of Hawaii at Manoa. Once a mutation was identified, it was confirmed in four more mice each of both +/+ and *rc*/*rc* genotypes from different parents, and in heterozygous (+/*rc*) mice. We also confirmed the mutation in B6/J-*rc* genomic DNA purchased from the Jackson Laboratory (Bar Harbor, ME) and in PCR-amplified cDNA generated from *rc*/*rc* mouse skin RNA. Sequence analysis of the mutated gene was also carried out on genomic DNA extracted from BALB/cJ, CAST/Ei, C3H/HeJ mice (The Jackson Laboratory, Bar Harbor, ME), B6C3F1, B6D2F1, CD1, and SwissGP mice (NCI-Frederick Animal Production Area, Frederick, MD), and C3H/HeJ-*ruf* genomic DNA purchased from the Jackson Laboratory (Bar Harbor, ME).

## RNA extraction and RT-PCR analysis:

The dorsal skin of euthanized B6/J-*rc*/*rc* and age- and sex-matched B6/J-+/+ mice was shaved, and skin biopsies as well as the internal organs were collected. Samples were frozen immediately in liquid nitrogen or immersed in RNA*later* (Qiagen, Valencia, CA). Total RNA was extracted using TriReagent (Molecular Research Center, Inc., Cincinnati, OH) following manufacturer's manual. Total RNA was reverse transcribed using the SuperScript III Reverse Transcriptase Kit (Invitrogen Corp., Carlsbad, CA). The first strand cDNA was used as templates for PCR amplification. The quality of the cDNA was confirmed by PCR amplification of glyceraldehyde-3-phosphate dehidrogenase cDNA analyzed by agarose gel electrophoresis.

## Antibody generation

Two rabbits were immunized with synthesized peptide DKLTIDWTYRPPSSSRT (amino acids 63~79, in the predicted extracellular domain of the murine MPZL3 protein), and the serum was affinity purified for antibodies against the peptide (Bethyl Laboratories, Montgomery, TX).

## Western blot analysis and indirect immunofluorscence

The full coding sequences of the wild type murine Mpzl3 cDNA, as well as

Mpzl3 cDNA harboring the rc mutation, were subcloned into the Pst I/Not I sites of pEF/myc/cyto (Invitrogen Corp., Carlsbad, CA), so that the Myc tag was at the carboxyl terminus of the fusion protein. The resulting plasmids were transfected into NIH/3T3 cells (ATCC, Manassas, VA) using LipofectAmine 2000 (Invitrogen Corp.), and the total cellular proteins were extracted using modified RIPA buffer (50mM Tris-Cl, pH7.4, 1mM each of EDTA, PMSF, $Na_3VO_4$ and NaF, 1% NP-40, 62.5mM each of ALLN and N-Etylmaleimide, and 1:15 diluted Protease Inhibitor cocktail). Biopsies of adult mouse skin were homogenized and the proteins extracted as described (He et al., 2002). Protein extracts were analyzed by gradient (Invitrogen Corp.) or non-gradient SDS-PAGE and blotted onto Immobilon transfer membrane (Millipore Corporation, Billerica, MA) for Western blot analysis following standard protocols. The molecular weight marker used was MagicMark XP (Invitrogen Corp.). The rabbit anti-MPZL3 antibodies were diluted 1:400 and mouse anti-Myc tag antibody (Covance Research Products, Princeton, NJ) was diluted 1:200. For antibody preabsorption, the rabbit anti-MPZL3 antibodies were incubated with excess peptide DKLTIDWTYRPPSSSRT at 1:3, 1:10, or 1:32 molar ratio for 1 hour before being added to the blot. Antibody binding was detected with ECL Western Blot Detection Reagents (GE Healthcare Bio-Sciences Corp., Piscataway, NJ) and BioMax film (Eastman Kodak Company, Rochester, NY). Cryosections of back skin biopsies of normal and rc/rc mice were incubated with 1:200 dilutions of rabbit anti-MPZL3 antibodies or normal goat serum. Antibody binding was detected with goat anti-rabbit IgG conjugated with FITC, and the slides were mounted in VectorShield with propidium iodide (Vector Laboratories, Burlingame, CA). The sections were examined and photographed on a Zeiss AxioSkop 2 Plus fluorescent microscope or a Zeiss 5 PASCAL LSM confocal microscope (Carl Zeiss MicroImaging, Inc., Thornwood, NY).

## Acknowledgments

This work was supported by grants AR047713 (KC) and AR050487 (TC) from NIH/NIAMS and G12RR003061 (KC, TC) from NIH/NCRR (RCMI program), and the Ingeborg v.F. McKee Fund from the Hawai'i Community Foundation (20040450 and 20050401 to TC). The authors would like to thank Scott Lozanoff, Charles D. Boyd, Yusuke Marikawa, Olivier Le Saux, Athula Wikramanayake's laboratory, Yvonne Tatsumura, Keith S. Fong, Xiao-Jing Wang's laboratory (Oregon Health and Science University), Dennis R. Roop and Paul A. Overbeek (Baylor College of Medicine) for helpful suggestions, Shannon Bennett and Durrell Kapan for help in linkage analysis, and Darlene Ramones and Marisa Tricas for technical assistance. Sequencing analyses were carried out at the CGPBRI, GMBF, and MBSR Sequencing Core Facilities at UHM, and microscopic images were captured and analyzed at the RCMI Imaging Core Facility. The GenBank accession number for murine Mpzl3 gene/mRNA is EF102773.